INTERNATIONAL JOURNAL FOR NUMERICAL METHODS IN ENGINEERING
Int. J. Numer. Meth. Engng 2012; **89**:991–1008
Published online 25 August 2011 in Wiley Online Library (wileyonlinelibrary.com). DOI: 10.1002/nme.3273

An interface-enriched generalized FEM for problems with discontinuous gradient fields

Soheil Soghrati[1], Alejandro M. Aragón[1], C. Armando Duarte[1] and Philippe H. Geubelle[2,3,*,†]

[1]*Department of Civil and Environmental Engineering, University of Illinois at Urbana-Champaign, Urbana, IL 61801, U.S.A.*
[2]*Beckman Institute of Advanced Science and Technology, University of Illinois at Urbana-Champaign, Urbana, IL 61801, U.S.A.*
[3]*Department of Aerospace Engineering, University of Illinois at Urbana-Champaign, Urbana, IL 61801, U.S.A.*

SUMMARY

A new generalized FEM is introduced for solving problems with discontinuous gradient fields. The method relies on enrichment functions associated with generalized degrees of freedom at the nodes generated from the intersection of the phase interface with element edges. The proposed approach has several advantages over conventional generalized FEM formulations, such as a lower computational cost, easier implementation, and straightforward handling of Dirichlet boundary conditions. A detailed convergence study of the proposed method and a comparison with the standard FEM are presented for heat transfer problems. The method achieves the optimal rate of convergence using meshes that do not conform to the interfaces present in the domain while achieving a level of accuracy comparable to that of the standard FEM with conforming meshes. Various application problems are presented, including the conjugate heat transfer problem encountered in microvascular materials. Copyright © 2011 John Wiley & Sons, Ltd.

Received 8 March 2011; Accepted 26 June 2011

KEY WORDS: GFEM/XFEM; heat transfer; convection-diffusion equation; gradient discontinuity; enrichment functions; microvascular materials

1. INTRODUCTION

Several problems in materials science and engineering include solution fields that are C^0–continuous. Classical examples include thermal or structural fields in composite materials where the difference in material properties between the phases leads to discontinuities in the gradient field, also known as weak discontinuities [1,2]. Another example can be found in the mesoscale modeling of polycrystalline materials where the mismatch in material properties at grain boundaries leads to a discontinuous gradient field [3]. In the general case, the mismatch between the phases involves not only the difference between material properties but also the effective terms in the governing differential equation based on the type of materials, for example, conjugate fluid/solid problems. Active cooling of materials through embedded microvascular networks [4] is an example of such problems, where, in addition to material properties, the effect of the convection in the fluid phase must be incorporated in the numerical solution.

An accurate FEM solution for such problems can only be achieved by adopting a conforming mesh, that is, a mesh that conforms to the interface geometry. In this case, the inherent gradient discontinuity between adjacent finite elements in the standard FEM accurately represents the weak

*Correspondence to: Philippe H. Geubelle, Beckman Institute of Advanced Science and Technology, University of Illinois at Urbana-Champaign, 405 North Mathews Avenue, Urbana, IL 61801 U.S.A.
†E-mail: geubelle@illinois.edu

discontinuity at the material interface. However, creating a conforming mesh that can appropriately represent the actual geometry of the structure while yielding elements with acceptable aspect ratios is a complex and often expensive process. Moreover, in some cases such as transient or optimization problems, where the geometry of the problem is changing throughout the analysis, the use of conforming meshes may simply be impossible [5, 6].

The aforementioned limitations of the standard FEM in handling problems with weak or strong discontinuities, where the latter refers to discontinuities in the solution field, have motivated the development of special numerical techniques. Among the most promising related methods is the generalized FEM (GFEM)/eXtended FEM (XFEM) [7–10], which aims at providing independence between the problem morphology and the finite element mesh used in the numerical solution. This is achieved by incorporating an a priori knowledge of the solution field in the form of enrichment functions at the nodes of elements cut by the the interface. Thus, despite the inherent geometrical complexity for determining the location of elements with respect to interface edges in two-dimensional or surfaces in three-dimensional, these methods provide a great simplification in modeling discontinuous phenomena with nonconforming meshes.

Early contributions to the GFEM/XFEM were directed towards linear elastic fracture mechanics and crack growth simulations [11–15]. Later contributions to the developement of GFEM/XFEM for this type of problems can be found in [16–19]. The implementation of these methods also gained interest in other areas addressing problems with weak and strong discontinuities. Such areas can be categorized but not limited to contact problems [14, 20], multiscale problems [21], multiphase/solidification [22, 23], and material or phase interfaces [24–26]. The current work focuses on the latter type of problems by introducing new enrichment functions and a different approach for applying them at the interface. In the proposed method, the generalized degrees of freedom (dofs) are not applied to nodes of the original mesh but are considered at the nodes that are created by intersecting the phase interface with element edges. Because the generalized dofs in this approach are applied to the interface nodes, we refer to the method as *interface GFEM* (IGFEM).

The remainder of the paper is organized as follows. In the next section, we discuss the formulation of the model problem that motivated this work, that is, the convection-diffusion equation, and the corresponding GFEM formulation. In Section 3, we introduce the enrichment functions used in the IGFEM and explain its formulation for solving the model problem with three-node triangular elements. Also, implementation issues of the IGFEM are discussed and compared with those of more conventional GFEM formulations for which generalized dofs are applied to the nodes of the original mesh. It must be noted that the application of the IGFEM is not limited to the convection-diffusion equation and can be easily extended to other problems (such as structural problems) with weak discontinuities. A detailed convergence study for this method is provided in Section 4 by comparing the accuracy and convergence rates with those of the standard FEM. We then apply the IGFEM to solve heat transfer problems in heterogeneous and actively cooled microvascular materials in Section 5.

2. PROBLEM DESCRIPTION

Consider an open domain $\Omega = \Omega_s \cup \Omega_f \subset \mathbb{R}^2$, $\Omega_s \cap \Omega_f = \emptyset$, composed of two mutually exclusive solid (Ω_s) and fluid (Ω_f) regions, with closure $\overline{\Omega}$ as shown in Figure 1. The boundary $\Gamma = \overline{\Omega} - \Omega$ has an outward unit normal $\mathbf{n}$ and is divided into three distinct partitions Γ_u, Γ_q, and Γ_h such that $\Gamma = \overline{\Gamma_u \cup \Gamma_q \cup \Gamma_h}$ and $\Gamma_u \cap \Gamma_q \cap \Gamma_h = \emptyset$. The strong form of the convection-diffusion boundary value problem can then be expressed as follows: Given the thermal conductivity $\boldsymbol{\kappa} : \overline{\Omega} \to \mathbb{R}^2 \times \mathbb{R}^2$, fluid density $\rho : \Omega_f \to \mathbb{R}$, fluid specific heat $c_p : \Omega_f \to \mathbb{R}$, velocity field $\mathbf{v} : \Omega_f \to \mathbb{R}^2$, heat source $f : \Omega \to \mathbb{R}$, and heat transfer coefficient $h : \Gamma_h \to \mathbb{R}$, find $u : \overline{\Omega} \to \mathbb{R}$ such that

$$\begin{aligned} -\nabla \cdot (\boldsymbol{\kappa} \nabla u) &= f && \text{on } \Omega_s, \\ -\nabla \cdot (\boldsymbol{\kappa} \nabla u) + \rho c_p \mathbf{v} \cdot \nabla u &= f && \text{on } \Omega_f, \\ u &= \bar{u} && \text{on } \Gamma_u, \\ \boldsymbol{\kappa} \nabla u \cdot \mathbf{n} &= q && \text{on } \Gamma_q, \\ \boldsymbol{\kappa} \nabla u \cdot \mathbf{n} &= h\,(u_\infty - u) && \text{on } \Gamma_h, \end{aligned} \tag{1}$$

DOI: 10.1002/nme

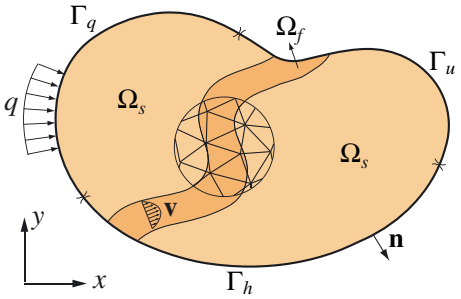

Figure 1. Schematic configuration of the geometry and boundary conditions of the domain used for heat transfer problems. The domain Ω is divided into two mutually exclusive regions Ω_{f} and Ω_{s}, corresponding to fluid and solid phases, respectively. The boundary Γ with outward unit normal $\mathbf{n}$ is composed of three distinct regions Γ_u, Γ_q, and Γ_h, corresponding to applied Dirichlet, Neumann, and Robin boundary conditions, respectively. The picture also illustrates a subset of a FEM mesh that does not conform to the phase interfaces in the domain.

where $\bar{u} : \Gamma_u \to \mathbb{R}$ is the prescribed temperature and $q : \Gamma_q \to \mathbb{R}$ the heat flux, that is, the Dirichlet and Neumann boundary conditions, respectively. Also, $u_\infty : \Gamma_h \to \mathbb{R}$ is the ambient temperature used in the evaluation of the Robin (convective) boundary conditions. It must be noted that if $\Omega = \Omega_{\mathrm{s}}$, that is, no fluid phase, or $\mathbf{v} = \mathbf{0}$, the model problem reduces to the Poisson equation.

Given the function spaces $\mathcal{U}$ and $\mathcal{V}$, defined as $\mathcal{U} \subset H^1\left(\overline{\Omega}\right) = \{u : u|_{\Gamma_u} = \bar{u}\}$ and $\mathcal{V} \subset H^1\left(\overline{\Omega}\right) = \{v : u|_{\Gamma_u} = 0\}$, the weak formulation of (1) is written as follows: Find $u \in \mathcal{U}$ such that

$$a\left(u, v\right) + a\left(u, v\right)_{\Gamma_h} = \left(v, f\right) + \left(v, q\right)_{\Gamma_q} + \left(v, u_\infty\right)_{\Gamma_h} \qquad \forall v \in \mathcal{V}, \tag{2}$$

where the linear and bilinear forms appearing in (2) are given by

$$\begin{aligned}
a\left(u, v\right) &= \int_\Omega \nabla v \cdot \left(\boldsymbol{\kappa} \nabla u\right)\, \mathrm{d}\Omega + \int_{\Omega_{\mathrm{f}}} v \rho c_p \mathbf{v} \cdot \nabla u \, \mathrm{d}\Omega, \\
a\left(u, v\right)_{\Gamma_h} &= \int_{\Gamma_h} h v u \, \mathrm{d}\Gamma_h, \\
\left(v, f\right) &= \int_\Omega v f \, \mathrm{d}\Omega, \\
\left(v, q\right)_{\Gamma_q} &= \int_{\Gamma_q} v q \, \mathrm{d}\Gamma_q, \\
\left(v, u_\infty\right)_{\Gamma_h} &= \int_{\Gamma_h} h v u_\infty \, \mathrm{d}\Gamma_h.
\end{aligned}$$

Selecting the subspaces $\mathcal{U}^h \subset \mathcal{U}$ and $\mathcal{V}^h \subset \mathcal{V}$ such that

$$\mathcal{V}^h = \left\{v^h \,:\, v^h|_{\Gamma_u} = 0\right\}, \mathcal{U}^h = \left\{u^h \,:\, u^h = v^h + t^h \,,\; t^h|_{\Gamma_u} = \bar{u} \,,\; v^h \in \mathcal{V}^h\right\},$$

the Galerkin formulation of (2) can be written as: Find $u^h \in \mathcal{U}^h$ such that

$$a\left(u^h, v^h\right) + a\left(u^h, v^h\right)_{\Gamma_h} = \left(v^h, f\right) - a\left(v^h, t^h\right) + \left(v^h, q\right)_{\Gamma_q} + \left(v^h, u_\infty\right)_{\Gamma_h} \quad \forall v^h \in \mathcal{V}^h. \tag{3}$$

Equation (3) can be directly used as the standard FEM approximation by discretizing the domain Ω into m finite elements ($\Omega \cong \Omega^h \equiv \cup_{i=1}^m \overline{\Omega_i}$) and by employing a set of n standard Lagrangian shape functions $N_i\left(\mathbf{x}\right)$ for approximating the field in each element such that

$$u^h\left(\mathbf{x}\right) = \sum_{i=1}^{n} N_i\left(\mathbf{x}\right) u_i. \tag{4}$$

DOI: 10.1002/nme

If a nonconforming mesh, as shown in Figure 1, is adopted, the Galerkin method is not capable to capture the gradient discontinuity at the interfaces, which introduces a substantial error and therefore a loss of the optimal rate of convergence. This problem can be addressed by enriching the solution space at the nodes of elements intersecting with the material interface to retrieve the missing information in the standard FEM solution. Within the GFEM framework, this can be done by using a set of local enrichment functions $\left\{\varphi_{ij}\left(\mathbf{x}\right):\mathbf{x}\rightarrow\mathbb{R}\mid N_i\left(\mathbf{x}\right)\neq 0\right\}_{j=1}^{n_{\text{en}}}$ where n_{en} is the number of enrichment functions associated with node i. The approximation of the solution field through the GFEM is then expressed as

$$u^h\left(\mathbf{x}\right)=\sum_{i=1}^{n}N_i\left(\mathbf{x}\right)\tilde{u}_i+\sum_{i=1}^{n}N_i\left(\mathbf{x}\right)\sum_{j=1}^{n_{\text{en}}}\varphi_{ij}\left(\mathbf{x}\right)\hat{u}_{ij}. \tag{5}$$

The first term of (5) is similar to the standard FEM approximation except for the fact that $\tilde{u}_i$ does not, in general, represent the field value at node i because of the presence of the second term in (5), which is associated with the contribution of enrichment functions in evaluating the nodal values of the solution. These enrichment functions are multiplied by the standard Lagrangian shape functions to provide a sparse resulting system of linear equations. It is worth mentioning that, although (5) seems to indicate that all nodes are enriched, this does not have to be the case in general.

Several issues are raised by the implementation of the GFEM formulation described by (5). The first issue involves handling the Dirichlet boundary conditions at the enriched nodes of the mesh. Based on (5), the field value at node i is given by $u_i=\tilde{u}_i+\sum_{j=1}^{n_{\text{en}}}\varphi_{ij}\left(\mathbf{x}_i\right)\hat{u}_{ij}$. Because both $\tilde{u}_i$ and $\hat{u}_{ij}$ are unknown values, the prescribed value of the solution field cannot be directly assigned to the enriched node. Instead, one must employ techniques such as the penalty method or Lagrange multipliers to enforce Dirichlet boundary conditions [27,28]. One could shift φ_{ij} such that it is zero at the nodes. But, the enforcement of boundary conditions between the nodes is still problematic. It is worth mentioning that for some enrichment functions such as those proposed in [26], the value of the enrichment function vanishes at the nodes; hence, enforcing the Dirichlet boundary conditions in the GFEM is as straightforward as in the standard FEM.

Another issue associated with the implementation of the GFEM involves in the blending of representing elements, that is, elements with attached enrichment to all nodes, to conventional finite elements. The problem arises because only some of the nodes in the blending elements are enriched; thus, the enrichment functions are not fully reproduced through the interpolation with Lagrangian shape functions described by (5). Hence, the incomplete terms of the enrichment functions added to the numerical approximation in such elements may, in fact, deteriorate the accuracy and rate of convergence. For linear interpolations, a solution is presented in [29] where all the nodes of blending elements are enriched through the implementation of corrective enrichment functions. However, as described in [25], higher-order interpolations do not have the aforementioned problem, and optimal rates of convergences are recovered.

The last implementation issue that we study here is the quadrature of enriched elements in the GFEM. Because of the inherent weak discontinuities in these functions, using the same order of Gauss points as that used in the standard FEM in these elements leads to a considerable error and degradation of the rate of convergence. It has also been shown that using higher-order Gauss quadratures in this case performs poorly in improving the accuracy [30]. Among several approaches proposed to address this problem, one of the most commonly accepted techniques consists in subdividing the element into subdomain elements and moving the standard quadrature from the parent element into these so-called *integration elements* [12, 13]. The only constraint on creating integration elements is that their boundaries must be aligned with discontinuity edges or surfaces of the domain and their aspect ratio does not affect the accuracy of the solution. As will be explained in the next section, the IGFEM addresses some of the implementation issues associated with the GFEM.

3. IGFEM: FORMULATION AND IMPLEMENTATION

To explain the basic idea behind the IGFEM formulation, we first study two different approaches for interpolating the solution field in a bimaterial domain, as shown in Figure 2. The standard FEM

DOI: 10.1002/nme

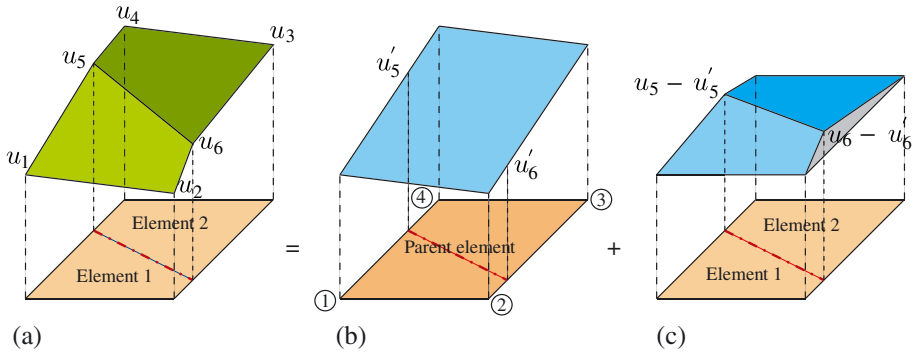

Figure 2. Two equivalent approaches for capturing the weak discontinuity at the phase interface (shown by a dash-dotted line) with Lagrangian shape functions: (a) standard FEM interpolation with two conforming elements, (b) interpolation with one nonconforming element, and (c) missing part of the field interpolation with the nonconforming element given in Figure (b).

interpolation of the field when the domain is divided into two conforming elements is depicted in Figure 2(a). Assuming that the nodal values of the field u_i are given and that elements are locally numbered counterclockwise starting from the lower left node (Figure 2(b)), the interpolation of the field using the Lagrangian shape functions in each element is given by

$$\begin{aligned} u^h = & N_1^{(1)} u_1 + N_2^{(1)} u_2 + N_3^{(2)} u_3 + N_4^{(2)} u_4 \\ & + \left(N_4^{(1)} + N_1^{(2)} \right) u_5 + \left(N_3^{(1)} + N_2^{(2)} \right) u_6, \end{aligned} \tag{6}$$

where $N_i^{(j)}$ denotes the standard Lagrangian shape function associated with the ith node of element j.

On the other hand, if the two elements are merged to form one nonconforming element, the field approximation with bilinear shape functions in the parent element, $N_i^{(\mathrm{p})}$, looks like the one shown in Figure 2(b). In this case, the standard FEM interpolation is not able to reconstruct the gradient discontinuity at the material interface; hence, the values u'_5 and u'_6 at the intersection of the element edges with the interface are different from the given values u_5 and u_6. The missing part of the field in this interpolation can be retrieved, as shown in Figure 2(c). An interpolation of the solution field equivalent to that given in (6) is then obtained as

$$\begin{aligned} u^h = & N_1^{(\mathrm{p})} u_1 + N_2^{(\mathrm{p})} u_2 + N_3^{(\mathrm{p})} u_3 + N_4^{(\mathrm{p})} u_4 \\ & + \left(N_4^{(1)} + N_1^{(2)} \right) \left(u_5 - u'_5 \right) + \left(N_3^{(1)} + N_2^{(2)} \right) \left(u_6 - u'_6 \right), \end{aligned} \tag{7}$$

where $N_i^{(\mathrm{p})}$ denotes the standard Lagrangian shape functions in the parent element. The previous equation can be rewritten as

$$u^h = N_1^{(\mathrm{p})} u_1 + N_2^{(\mathrm{p})} u_2 + N_3^{(\mathrm{p})} u_3 + N_4^{(\mathrm{p})} u_4 + \psi_1 \alpha_1 + \psi_2 \alpha_2, \tag{8}$$

where, similar to the GFEM formulation, $\psi_1 = N_4^{(1)} + N_1^{(2)}$ and $\psi_2 = N_3^{(1)} + N_2^{(2)}$ are considered as enrichment functions and α_1 and α_2 are interpreted as generalized dofs. We can then extend (8) into the formulation of the IGFEM as

$$u^h(\mathbf{x}) = \sum_{i=1}^{n} N_i(\mathbf{x}) u_i + \sum_{i=1}^{n_{\mathrm{en}}} s \psi_i(\mathbf{x}) \alpha_i, \tag{9}$$

where the coefficient s is a scaling factor that will be introduced later.

Several important characteristics of the IGFEM can be observed by comparing (9) with the formulation of the conventional GFEM in (5). Similar to the conventional GFEM, the first term of

DOI: 10.1002/nme

(9) represents the standard FEM portion of the approximation. However, unlike the conventional GFEM, the coefficients associated with the first term in the IGFEM directly correspond to the values of the field at each node. The second term in (9) denotes the effect of the enrichment functions in the solution field because the enrichment functions vanish at these locations. The main difference between this term and the corresponding term in (5) is the approach for assembling the generalized dofs. Although the partition of unity, that is, $\sum_{i=1}^{n} N_i(\mathbf{x}) = 1$, is used in the conventional GFEM to paste together the enrichment functions, a unified enrichment in the IGFEM is achieved by sharing the same generalized dofs between interface nodes of adjacent elements and not nodes of the original mesh. Figure 3 presents a schematic view of the portion of the IGFEM solution constructed by the enrichment functions and shows how these functions are stitched together over the material interface. As also shown in the schematic, if an interface node coincides with one of the nodes of the original mesh, no enrichment is attached to that node. This is because the standard FEM portion of the approximation in (9) directly yields the values of the field at the nodes of the original mesh. Hence, the proposed enrichment functions vanish at the location of the node, and it is not necessary to enrich such nodes. It must be noted that because of the special approach used for applying the enrichment functions in the IGFEM, this method can be also considered as an *h-hierarchical* approach [31].

3.1. Enrichment functions

Referring back to (7) and (8), the enrichment functions used for interpolating the solution field in Figure 2 were obtained as the sum of Lagrangian shape functions in the two conforming elements. This approach can be extended in the IGFEM formulation through selecting appropriate Lagrangian shape functions in the integration elements and using their linear combination as the enrichment function. In order to evaluate the enrichment functions for triangular elements, we first divide the elements intersecting with the phase interface into the minimum number of integration elements required to obtain accurate quadrature. The enrichment function corresponding to an interface node is then constructed as the linear combination of the Lagrangian shape functions in the integration elements with a unity value at that node. The integration elements and enrichment functions for two possible orientations of a triangular element with respect to the phase interface are presented in Figure 4. As shown in this figure, the parent element is divided into either two triangular elements or one triangular and one quadrilateral element based on the position of the phase interface. It must be noted that evaluating the enrichment functions in quadrilateral elements is similar: first, divide the element into two triangular subelements, and then let each triangular element interact with the interface and enrich them as explained. These triangular subelements are only generated for the evaluated enrichment functions, and the shape functions used in the first term of (9) are still obtained from quadrilateral elements.

As mentioned before, the aspect ratio of integration elements in the GFEM, and similarly in the IGFEM, does not affect the accuracy of the solution. However, because enrichment functions in the IGFEM are created from the Lagrangian shape functions associated to the integration elements, numerical difficulties arise if an interface node is too close to one of the nodes of the parent element.

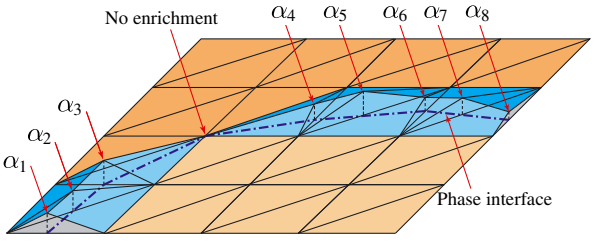

Figure 3. Contribution of enrichment function for modeling the weak discontinuity in the interface generalized FEM. The generalized dof α_i denotes how the enrichment functions are stitched together over the interface nodes to provide a continuous enrichment. No enrichment is attached to an interface node if it coincides with one of the nodes of the original mesh.

DOI: 10.1002/nme

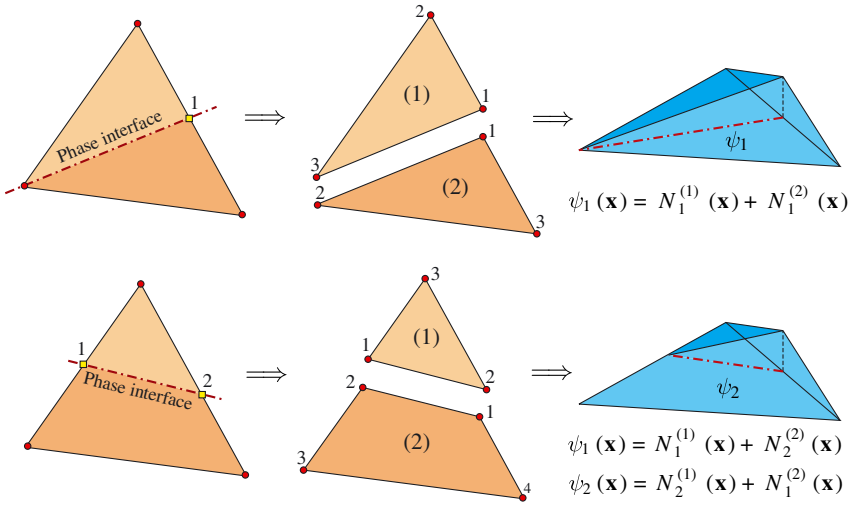

Figure 4. Evaluation of the enrichment functions in the interface generalized FEM: two scenarios for creating the integration elements and corresponding enrichment functions based on the location of the interface in the intersected triangular element.

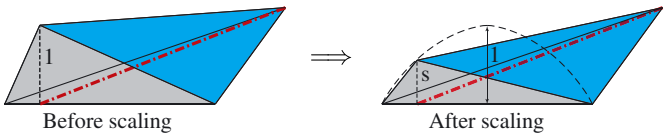

Figure 5. Scaling the enrichment functions using a parabolic function based on the distance between an interface node and nodes of the element's edge to avoid ill-conditioning. The dash-dotted line denotes the location of the interface.

In this case, the high aspect ratio of resulting integration elements and consequently the large gradient values of the corresponding enrichment functions may lead to the formation of an ill-conditioned stiffness matrix. In fact, this issue is a substantial problem in adaptive methods where creation of a conforming mesh from the original mesh is desired, and often, special techniques are required for handling the resulting ill-conditioned matrices [32].

To avoid the aforementioned problem, we can scale the enrichment functions to control their gradient values in the numerical solution [26]. It must be remembered that the closer an interface node is located to one of the nodes of the parent element, the smaller the corresponding coefficient α_i, appearing in (9). Thus, one can scale down the enrichment functions as the interface node gets closer to one of the nodes of the parent element's edge without affecting their performance in modeling the gradient discontinuity along the interface. In other words, instead of using the original enrichment functions in this case, which leads to a very large gradient value and yields a vanishing coefficient α_i, scaling down the enrichment function controls the gradient value while avoiding an excessively large value of α_i. The relative location of the intersection point along the edge of the element is quantified by

$$\epsilon := \frac{\min\left(\|\mathbf{x}_1 - \mathbf{x}_{\text{int}}\|, \|\mathbf{x}_2 - \mathbf{x}_{\text{int}}\|\right)}{\|\mathbf{x}_2 - \mathbf{x}_1\|}, \tag{10}$$

where $\mathbf{x}_1$ and $\mathbf{x}_2$ are the nodes defining the intersecting edge of the parent element with the interface and $\mathbf{x}_{\text{int}}$ is the intersection point over this edge. We then scale the enrichment function by factor $s = 4\epsilon^2$, appearing in (9), which is a parabolic function with a unity value in the middle of the element's edge and zero at its defining nodes (Figure 5). This scaling can be introduced for any value of ϵ, or only when it is below a chosen threshold (say, $\epsilon < 0.01$).

DOI: 10.1002/nme

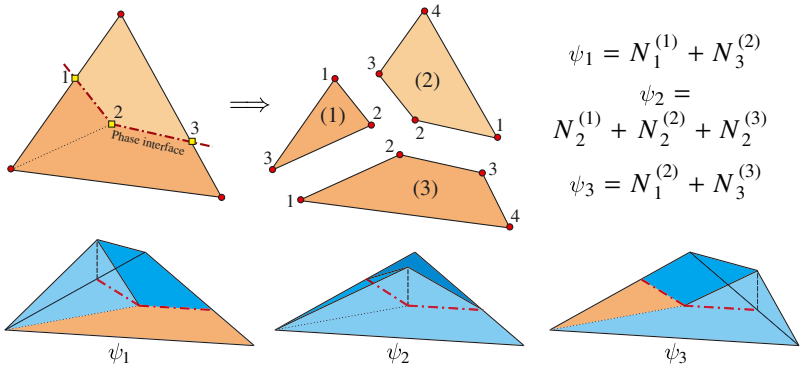

Figure 6. Creation of integration elements and evaluation of interface generalized FEM enrichment functions for a three-node triangular element cut by an interface made by two intersecting linear segments.

When a straight interface completely splits an element, the proposed IGFEM enrichment functions resemble the ridge enrichments proposed in [26], which were based on the level set method. Instead, the IGFEM uses a linear combination of the Lagrangian shape functions in the integration elements for constructing the enrichment functions. Also, in the IGFEM, the generalized dofs are attached to the interfaces nodes, and we no longer employ the partition of unity for attaching enrichment to the nodes of the original mesh.

Furthermore, the IGFEM provides more flexibility for evaluating the enrichment functions in elements cut by piecewise linear interfaces or interfaces intersecting within an element. For instance, consider a three-node triangular element cut by an interface defined by two intersecting linear segments as shown in Figure 6. Unlike the level set approach described in [26], the proposed IGFEM formulation is able to capture this type of interface geometry by dividing the parent element into the minimum number of integration elements needed for accurate quadrature and by using a linear combination of the Lagrangian shape functions in these elements to obtain the enrichment functions. We only need to add an interface node at the intersection point of the interface segments and add a generalized dof there to capture the gradient jump at this location. The integration elements and corresponding enrichment functions for the element cut by an interface with weak discontinuity are presented in Figure 6. The same approach can be easily extended for evaluating the enrichment functions in elements cut by three or more intersecting interfaces. Moreover, one can add one or more interface nodes over the interface inside an element, as shown in Figure 6, to reduce the geometry approximation errors associated with curved interfaces.

3.2. Implementation issues: Comparison with conventional GFEM

One of the unique features of the IGFEM is the way that enrichment functions are constructed through the linear combination of the Lagrangian shape functions of integration elements. It must be noted that, regardless of the type of enrichment functions used in the GFEM, evaluating the Lagrangian shape functions in the integration elements is essential for the Gaussian quadrature in the parent element, that is, for inverse mapping of the Gauss points in the integration elements to global coordinates of the parent element. Thus, a direct implementation of such shape functions as enrichment functions in the IGFEM reduces the computational cost and simplifies the implementation.

A key advantage of the IGFEM is the elimination of the aforementioned problems encountered in some GFEM formulations when applying Dirichlet boundary conditions at the enriched nodes. Because the generalized dofs in the IGFEM are assigned to the interface nodes and not to nodes of the original mesh, the process for applying Dirichlet boundary conditions in this method is similar to that of the standard FEM. Moreover, if an interface node is located over Γ_u (Figure 1), more information from the prescribed values of the field over the boundary can be incorporated into the numerical solution by prescribing the values of the generalized dofs at such nodes. This value can be

DOI: 10.1002/nme

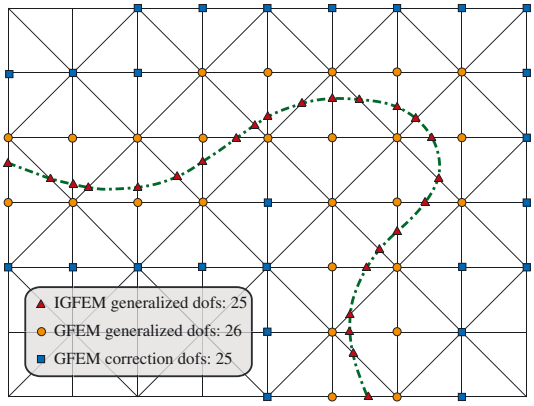

Figure 7. Required number of generalized dofs for IGFEM and conventional GFEM for a nonconforming mesh of three-node triangular elements. The triangular symbols denote the location of additional dofs introduced by the IGFEM over the interface (shown by dash-dotted line), whereas circles correspond to the nodes where the additional dofs are introduced with the conventional GFEM in the absence of correction. The additional dofs associated with the presence of a transitional region composed of blending elements are shown with squares.

easily determined by subtracting the standard FEM interpolation of the solution value over Γ_u using the given field values at the defining nodes of the edge of the parent element from the prescribed value of the solution at the interface node. Thus, for a nonconforming mesh, IGFEM provides a simple way to incorporate in the numerical solution the boundary values of the phase interface, whereas a similar direct approach is not suited for conventional GFEM.

To assess the computational cost of the IGFEM, we compare the associated number of dofs with that of the conventional GFEM. Figure 7 illustrates the required generalized dofs for solving a sample domain, discretized with three-node triangular elements, through both the conventional GFEM and IGFEM. As shown there, in the best-case scenario for the conventional GFEM where no correction [29] is needed in blending elements to achieve the optimal rate of convergence, the number of generalized dofs in this method is similar to that in the IGFEM. For GFEM formulations that require correction in the blending elements, the number of generalized dofs is much higher (twice for the domain shown in Figure 7).

4. CONVERGENCE STUDY

To investigate the convergence and accuracy of the IGFEM, the L_2-norm and H^1-norm of the error, defined as

$$\left\|u-u^h\right\|_{L_2(\Omega)}=\sqrt{\int_\Omega \left(u-u^h\right)^2 \mathrm{d}\Omega}, \tag{11}$$

$$\left\|u-u^h\right\|_{H^1(\Omega)}=\sqrt{\int_\Omega \left(u-u^h\right)^2+\left\|\nabla u-\nabla u^h\right\|^2 \mathrm{d}\Omega}, \tag{12}$$

are evaluated and compared with those of the standard FEM obtained with conforming meshes. Also, we investigate the effect of the shape of the phase interface and the material mismatch across the interface on the accuracy and rate of convergence of the numerical solution.

4.1. Example 1: gradient discontinuity along a straight interface

In the first example, we study the convergence rates of the IGFEM solution for the heat conduction problem shown in Figure 8(a) and compare it with that of the standard FEM. The solution field for

DOI: 10.1002/nme

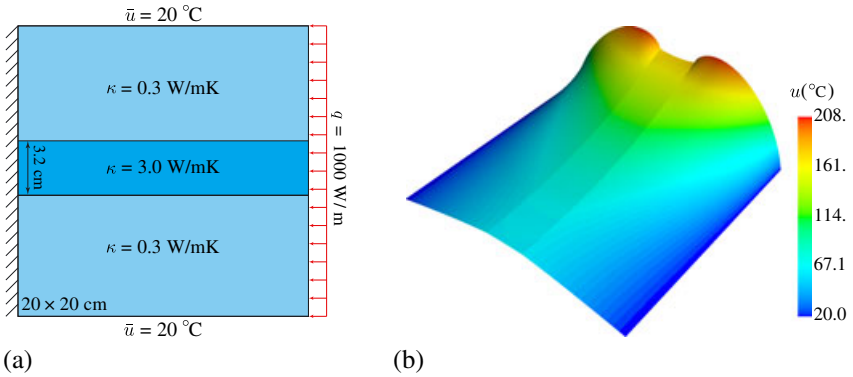

Figure 8. Domain, boundary conditions, and the solution field for the first example problem. The darker strip in the middle of the domain has a conductivity value 10 times larger than the rest of the domain, causing a discontinuous gradient along its edges.

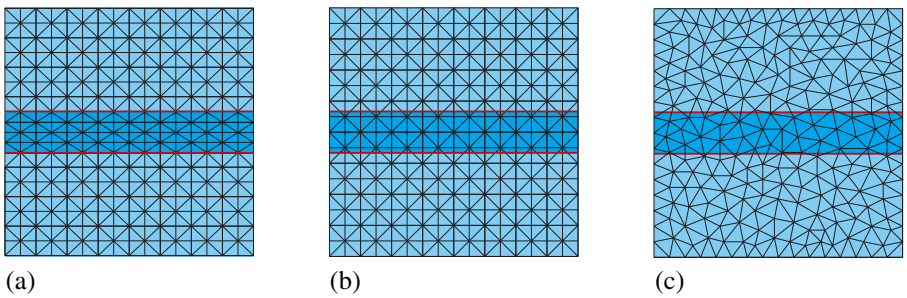

Figure 9. Three different types of meshes used for the numerical solutions in the first example problem: (a) structured conforming mesh for the standard FEM solution, (b) structured and (c) unstructured nonconforming meshes for the interface generalized FEM solution.

this problem is displayed in Figure 8(b). As shown there, the mismatch between conductivity values along the edges of the strip creates a spatially varying discontinuity in the gradient field.

To study the convergence of the IGFEM solution, the standard FEM solution with an extremely refined conforming mesh of six-node triangular elements outlined on a 2000×2000 grid is used as the reference solution. The IGFEM results are compared with those of the standard FEM obtained using structured conforming meshes with three-node triangular elements. Structured and unstructured nonconforming meshes are used in conjunction with the IGFEM, as illustrated in Figure 9.

The rates of convergence for the L_2-norm and H^1-norm of the error with respect to the mesh size and total number of dofs are presented in Figures 10 and 11, respectively. As observed in these figures, the IGFEM yields similar rates of convergence as that of the standard FEM without the need of conforming meshes. Moreover, the accuracy of the IGFEM results is often better than that of the standard FEM. It must be emphasized that this optimal rate of convergence is achieved without any correction in blending elements, which reduces both the cost and complexity of the implementation of this method.

4.2. Example 2: Curved interfaces and effect of material mismatch

The use of conforming meshes in problems with curved interfaces solved with the standard FEM does not usually yield optimal rate of convergence because of the geometry approximation error. Similarly, we do not expect to achieve the optimal rate of convergence for such problems using

DOI: 10.1002/nme

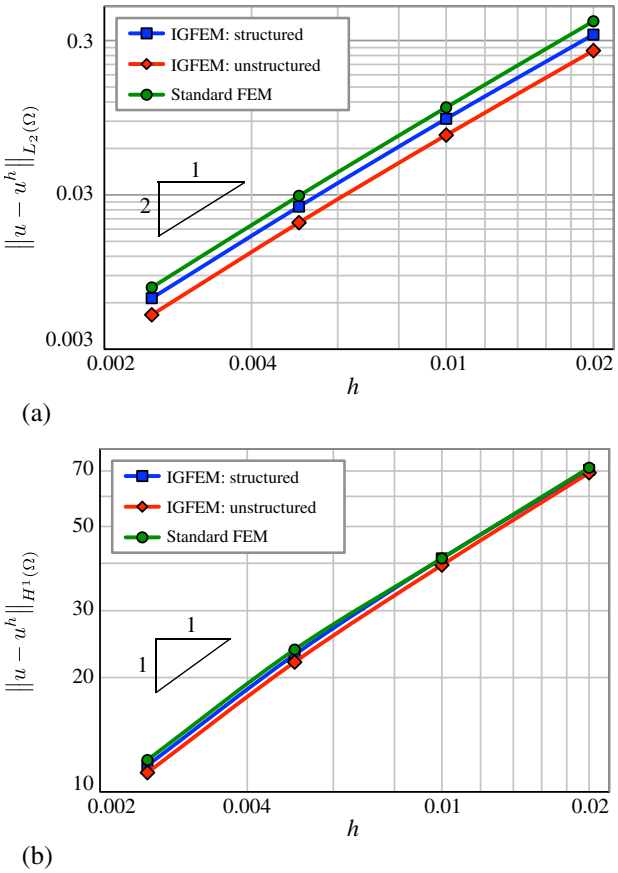

Figure 10. Convergence rates in L_2-norm and H^1-norm of the error with respect to the mesh size (h) for the example problem shown in Figure 8. Interface generalized FEM (IGFEM) results are obtained using structured and unstructured meshes similar to those shown in Figure 9.

the IGFEM. Instead, the goal here is to compare the performance of the IGFEM with that of the standard FEM to determine the efficiency of this method for handling such problems. The effect of the material mismatch, that is, the ratio of the thermal conductivity values across the interface, on the performance of the IGFEM is another issue studied in this example. It has been shown that the accuracy of conventional GFEM deteriorates when the conductivity mismatch increases, and further corrections are necessary to achieve the optimal rate of convergence [33].

The domain and boundary conditions for the second example problem are depicted in Figure 12(a). The material mismatch values are investigated corresponding to three values of the thermal conductivity ratio $\beta = \kappa_i/\kappa_m = 5, 50$, and 500, where κ_i and κ_m refer to the thermal conductivity of the inclusion and matrix, respectively. The corresponding thermal fields obtained with the IGFEM on a 40×40 unstructured nonconforming mesh are presented in Figures 12(b), 12(c), and 12(d), respectively, showing the ability of the IGFEM to capture the increasing gradient discontinuity across the interface.

Because no exact solution is available for this problem, a standard FEM solution obtained with a highly refined conforming mesh of 10-node triangular elements is used as the reference solution. The convergence rates for the L_2-norm and H^1-norm of the error for the standard FEM and IGFEM solutions are presented in Figure 13 for the three values of mismatch ratio α. As shown in this figure, the accuracy and convergence rates of the IGFEM solutions are similar and, in some cases, better than the corresponding results obtained with the standard FEM. It should also be noted that, without any correction, the performance of the IGFEM does not deteriorate as the conductivity values across the interface increases.

DOI: 10.1002/nme

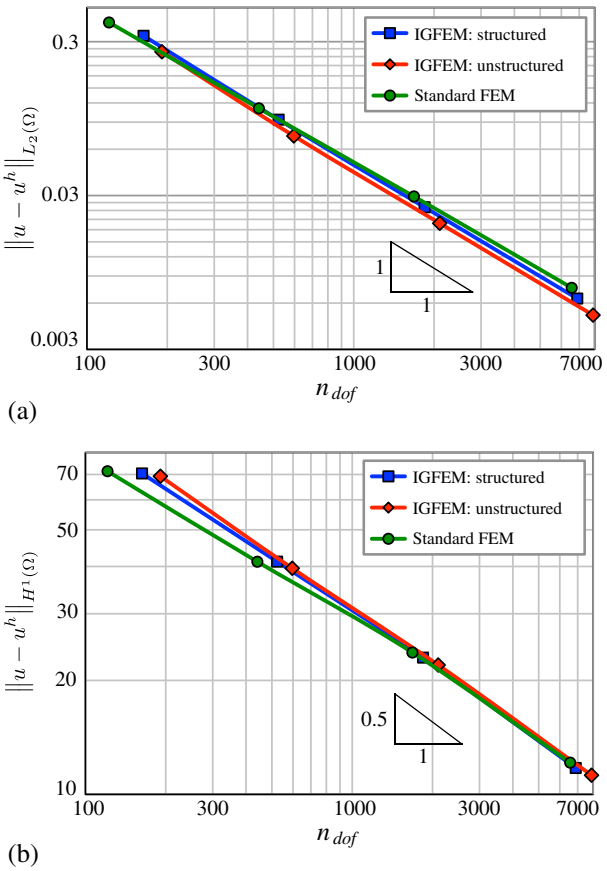

Figure 11. Convergence rates in L_2-norm and H^1-norm of the error with respect to the total number of dofs (n_{dof}) for the example problem shown in Figure 8. IGFEM, interface generalized FEM.

5. APPLICATIONS

In this section, we apply the IGFEM to solve two thermal problems with gradient discontinuity. We use these applications to address issues such as assigning Dirichlet boundary conditions at elements intersecting with the interface and conjugate heat transfer problems.

5.1. Application 1: heterogeneous material with multiple circular inclusions

The test problem shown in Figure 14(a) can be considered as a model problem for heat transfer in heterogeneous materials. Prescribed temperature boundary conditions with sinusoidal variations are considered along the top and bottom edges of the domain, whereas a constant heat flux is applied to the sides.

The IGFEM solution field shown in Figure 14(b) is obtained with a 120×80 nonconforming structured mesh of three-node triangular elements. The gradient discontinuity at material interfaces can be clearly distinguished in the IGFEM solution. As shown in Figure 14(a), some of the inclusions intersect the domain boundary with prescribed values of temperature. As discussed earlier in Section 3, assigning Dirichlet boundary conditions at nodes of the enriched elements in the IGFEM is similar to that of the standard FEM and requires no special modifications. Figure 14(b) clearly illustrates that the solution field along the boundaries with prescribed values of temperature is not affected by inclusions intersecting these boundaries and smoothly follows the prescribed sinusoidal values.

DOI: 10.1002/nme

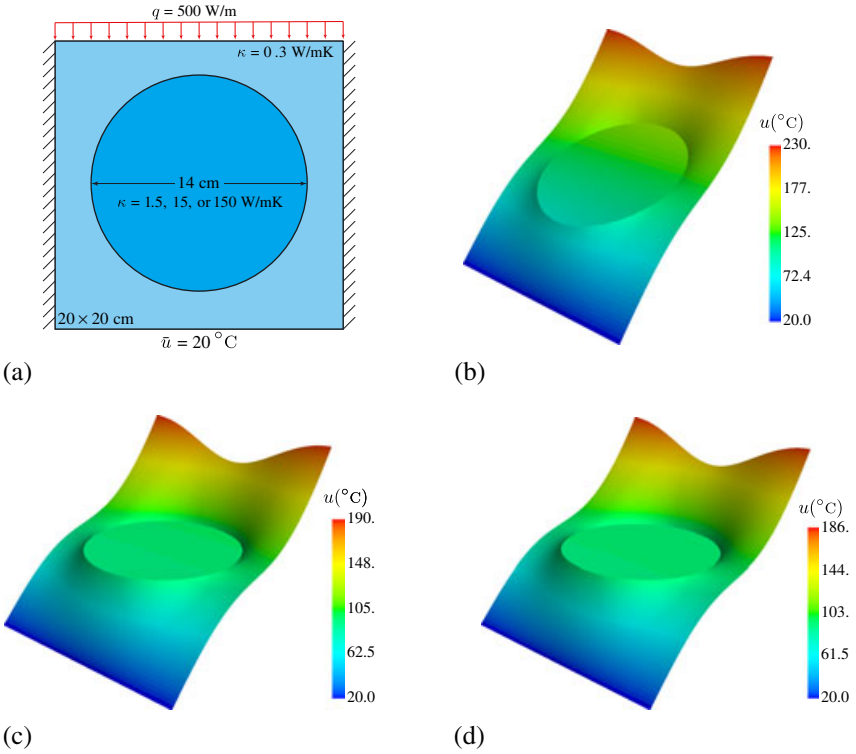

Figure 12. (a) Domain geometry and boundary conditions of the second example problem. The circular inclusion has a larger conductivity (κ_i) than the rest of the domain (κ_m). (b) Temperature field for $\alpha = \kappa_i/\kappa_m = 5$, (c) 50, and (d) 500.

5.2. *Application 2: Active cooling in microvascular materials*

The second application problem is motivated by the development of actively cooled microvascular polymers and polymer-based composites to be used in high-temperature applications. Recent advances in the manufacturing of embedded two-dimensional and three-dimensional microvascular networks using direct ink writing technique [34, 35] or the sacrificial fiber approach [36] have allowed the creation of a new class of materials and structures containing complex networks of microchannels (with diameters ranging from a millimeter down to a few microns) through which a coolant flows. By convecting the heat in these microchannels, these networks redistribute the heat in the microvascular medium and reduce its maximum temperature [37].

The model problem adopted in this example involves solving a conjugate heat transfer problem in a microvascular epoxy fin ($\kappa = 0.3$ W/m K) whose dimensions and thermal loading are depicted in Figure 15. The convective (Robin) boundary conditions along the left and right boundaries assume an ambient temperature of $u_\infty = 20$ °C and a heat transfer coefficient $h = 7.9$ W/m. The temperature is set to 15 °C along the bottom edge of the domain, and a uniform heat flux of 5768 W/m is applied along the top edge. This particular value is chosen so that the maximum temperature along the top edge of the domain in the absence of cooling is 150 °C.

Motivated by manufacturing constraints involved in the use of the sacrificial fiber technique, we adopt a sinusoidal shape for the centerline of the microchannel with amplitude $A = 3.2$ mm and diameter $D = 500$ μm. This particular configuration of the microchannel can be effectively used in active cooling of the domain with boundary conditions shown in Figure 15 through redistributing the heat inside the domain. The coolant used in this study is water ($\kappa = 0.6$ W/m K, $\rho = 1000$ kg/m^3, $c_p = 4183$ J/kg K), with an inflow temperature set at $u_e = 20$ °C and a mass flow rate $\dot{m} = 2$ g/min. Convective boundary conditions, similar to that of the surrounding matrix at the sides, is considered for the fluid at the outflow. Fully developed Poiseuille flow conditions are assumed in the microchannel, with a velocity profile given by [38]

DOI: 10.1002/nme

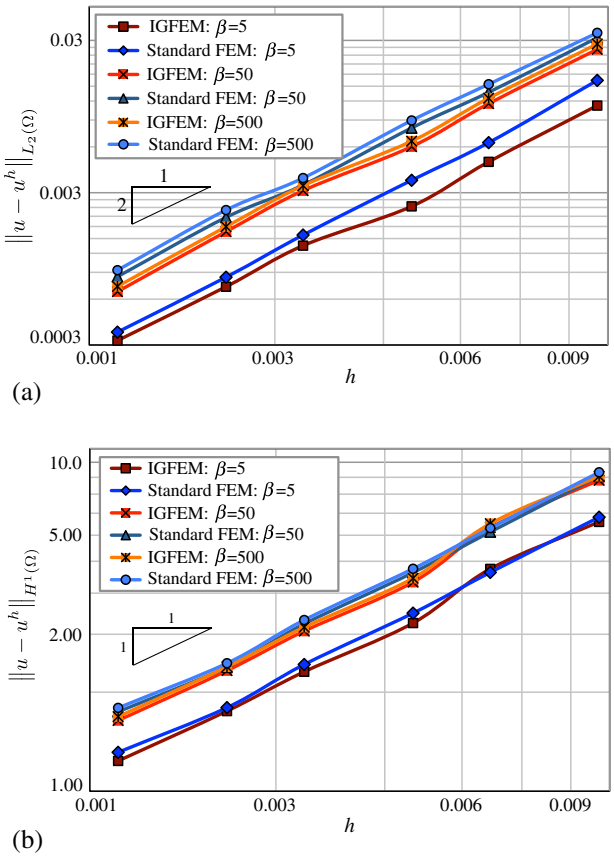

Figure 13. Convergence rates in L_2-norm and H^1-norm of the error with respect to the mesh size (h) for the second test problem shown in Figure 12(a). β denotes the thermal conductivity ratio across the material interface. IGFEM, interfaced generalized FEM.

$$|\mathbf{v}| = 2\overline{v}\left[1 - \left(\frac{2r}{D}\right)^2\right],$$

where $\overline{v} = 4\dot{m}/\pi D^2$ is the average velocity of the fluid and r is the radial distance from the centerline.

Details of the nonconforming mesh used in this study are shown in the inset of Figure 15. The domain is discretized with a structured mesh of three-node triangular elements outline over a 360×42 grid. The temperature field for this problem for three different wavelengths of the microchannel is presented in Figure 16. For the sake of clarity, the temperature profile inside the microchannels is not shown in this figure. However, Figure 16(d) shows the temperature profile along the line depicted in Figure 16(b) where the temperature distribution inside the microchannel and the weak discontinuity along its edges can be clearly observed.

One of the key design variables for this class of materials is the wavelength of the embedded sinusoidal microchannel. As shown in Figure 16, the wavelength plays an important role in redistributing the heat in the component as the coolant absorbs the heat from the hot area of the domain at the peaks of the sinusoidal curve and exchanges the heat in the colder region, that is, bottom of the domain, achieving a substantial reduction on the maximum temperature in the polymeric fin. This reduction is especially apparent in the embedded microchannel with the smaller wavelength (to the detriment, of course, of the additional cost of driving the fluid through a longer microchannel). It should be noted that the IGFEM is particularly well suited for this class of computational design, as the same mesh can be used to find the optimal configuration of the microvascular network.

DOI: 10.1002/nme

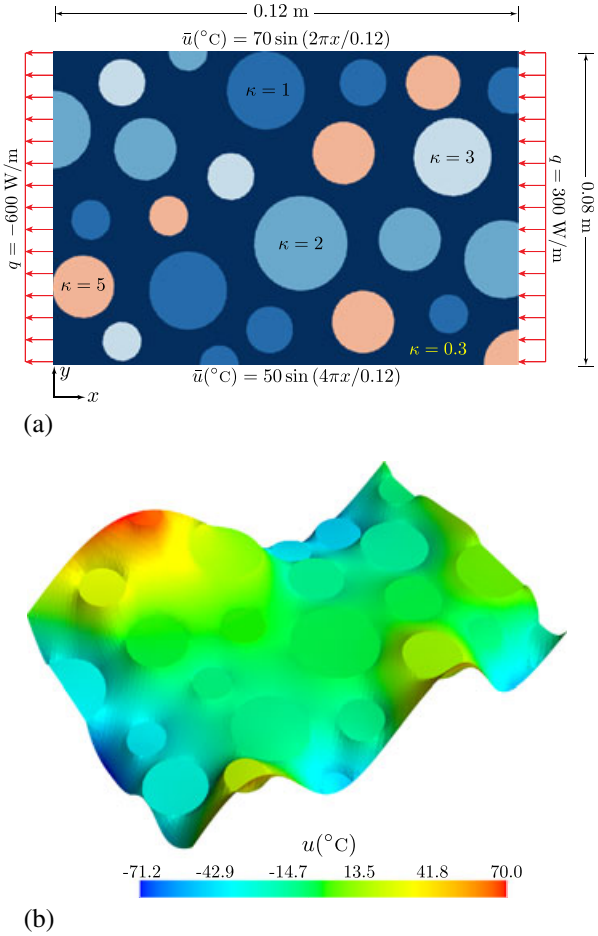

Figure 14. Problem statement and solution field obtained with the interfaced generalized FEM for the thermal problem in the model heterogeneous material. The shades or colors used in the inclusions and in the matrix correspond to prescribed values of the thermal conductivity given in W/m K.

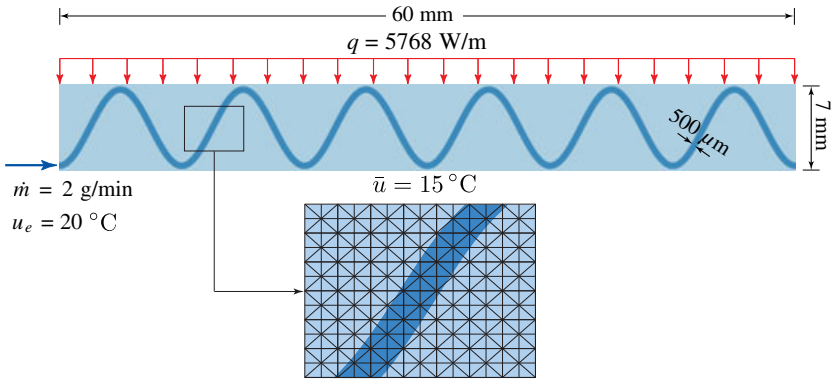

Figure 15. Domain geometry, boundary conditions, and schematic configuration of the sinusoidal microchannel for the second application problem. The domain is composed of epoxy material, and the fluid circulating in the microchannels is water. The inset shows a part of the structured nonconforming mesh used in the interfaced generalized FEM solution.

DOI: 10.1002/nme

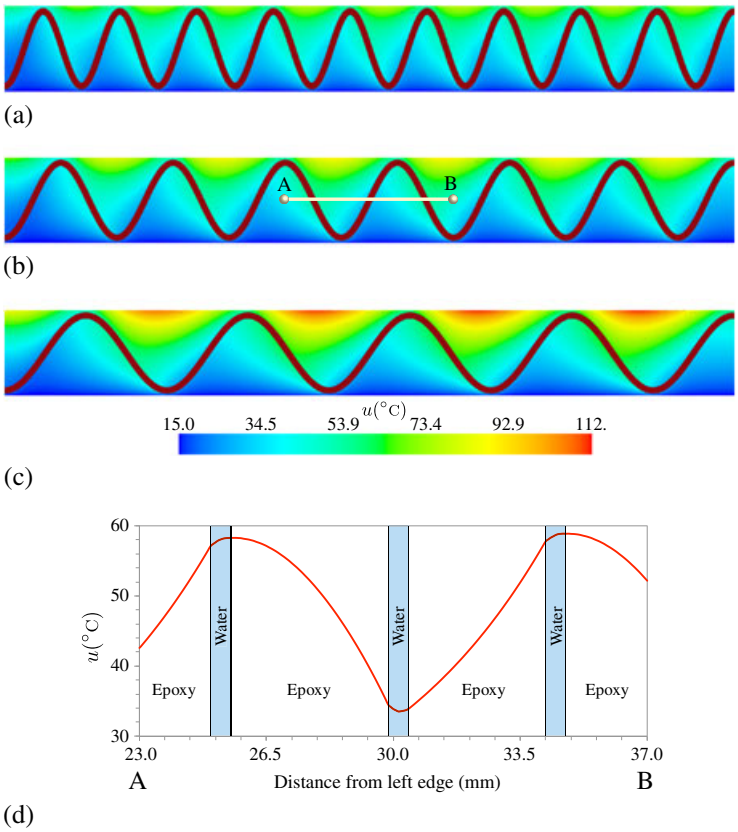

Figure 16. Interfaced generalized FEM solution for the second application problem presented in Figure 15: (a), (b), and (c) represent the temperature field in the actively cooled domain for a wavelength of the microchannel of 6.13, 9.23, and 13.33 mm, respectively. (d) Temperature profile along the line segment AB shown in Figure (b). The darker vertical regions denote the location of the microchannel.

6. CONCLUSIONS

The formulation and implementation of an interface-based GFEM scheme for solving thermal problems in discontinuous gradient fields has been presented. Similar to conventional GFEM, this new method can be used for solving problems with gradient discontinuity without using a conforming mesh. The unique feature of the IGFEM is that generalized dofs are assigned to the interface nodes and not to the nodes of the original FEM mesh. This variation in the formulation of the IGFEM eliminates problems encountered with some enrichment functions in the conventional GFEM for assigning Dirichlet boundary conditions at the enriched nodes. Moreover, enrichment functions in the IGFEM are simply constructed through the linear combination of standard Lagrangian shape functions of the integration elements, which reduces the cost and facilitates the implementation of this method. It was shown that the IGFEM solutions obtained with nonconforming meshes achieve the same optimal rate of convergence and level of accuracy as those of the standard FEM with conforming meshes. Moreover, unlike some GFEM formulations, the performance of the method is not deteriorated as the ratio of the material mismatch across the interface increases. We also investigated the application of the IGFEM for heat transfer in heterogeneous materials and conjugate heat transfer in actively cooled microvascular materials.

ACKNOWLEDGEMENTS

This work has been supported by the Air Force Office of Scientific Research Multidisciplinary University Research Initiative (Grant No. F49550-05-1-0346). The authors wish to thank insightful discussions with Prof. S. R. White, Prof. N. R. Sottos, and Dr. P. R. Thakre at the University of Illinois.

DOI: 10.1002/nme

REFERENCES

1. Song YS, Youn JR. Evaluation of effective thermal conductivity for carbon nanotube/polymer composites using control volume finite element method. *Carbon* 2006; **44**(4):710–717.
2. Wang XF, Zhou GM, Wang XW, Zhou CW. Multi-scale analyses of 3D woven bomposite based on periodicity boundary conditions. *Journal of Composite Materials* 2007; **41**(14):1773–1788.
3. Iuga M, Raether F. FEM simulations of microstructure effects on thermoelastic properties of sintered ceramics. *Journal of the European Ceramic Society* 2007; **27**:511–516.
4. Shipton LA. Thermal management applications for microvascular systems. *Master's Thesis*, University of Illinois at Urbana-Champaign, 2007.
5. Yue Z, Robbins DH Jr. Adaptive superposition of finite element meshes in non-linear transient solid mechanics problems. *International Journal for Numerical Methods in Engineering* 2007; **72**:1063–1094.
6. Canales J, Tarrago JA, Hernindez A. An adaptive mesh refinement procedure for shape optimal design. *Advances in Engineering Software* 1993; **18**:131–145.
7. Duarte CA, Oden TJ. Hp clouds–an hp meshless method. *Numerical Methods for Partial Differential Equations* 1996; **12**(6):673–705.
8. Oden TJ, Duarte CA, Zienkiewicz OC. A new cloud-based hp finite element method. *Computer Methods in Applied Mechanics and Engineering* 1998; **153**(1–2):117–126.
9. Melnek JM, Babuška I. The partition of unity finite element method: basic theory and applications. *Computer Methods in Applied Mechanics and Engineering* 1996; **139**(1–4):289–314.
10. Babuška I, Melnek JM. The partition of unity method. *International Journal for Numerical Methods in Engineering* 1997; **40**(4):727–758.
11. Duarte CA, Babuška I, Oden TJ. Generalized finite element methods for three-dimensional structural mechanics. *Computers and Structures* 2000; **77**(2):215–232.
12. Belytschko T, Black T. Elastic crack growth in finite elements with minimal remeshing. *International Journal for Numerical Methods in Engineering* 1999; **45**(5):601–620.
13. Moës N, Dolbow J, Belytschko T. A finite element method for crack growth without remeshing. *International Journal for Numerical Methods in Engineering* 1999; **46**(1):131–150.
14. Dolbow J, Moës N, Belytschko T. Discontinuous enrichment in finite elements with a partition of unity method. *Finite Elements in Analysis and Design* 2000; **36**:235–260.
15. Sukumar N, Moës N, Moran B, Belytschko T. Extended finite element method for three-dimensional crack modeling. *International Journal for Numerical Methods in Engineering* 2000; **48**:1549–1570.
16. Moës N, Belytschko T. Extended finite element method for cohesive crack growth. *Engineering Fracture Mechanics* 2002; **69**:813–833.
17. Mergheim J, Kuh E, Steinmann P. A finite element method for the computational modeling of cohesive cracks. *International Journal for Numerical Methods in Engineering* 2005; **63**:276–289.
18. Samaniego E, Belytschko T. Continuum–discontinuum modeling of shear bands. *International Journal for Numerical Methods in Engineering* 2005; **62**:1857–1872.
19. Song JH, Areias PMA, Belytschko T. A method for dynamic and shear band propagation with phantom nodes. *International Journal for Numerical Methods in Engineering* 2006; **67**:868–893.
20. Khoei AR, Nikbakht M. Contact friction modeling with the extended finite lement method (X-FEM). *Journal of Material Science Technology* 2006; **177**:58–62.
21. Fish J, Yuan Z. Multiscale enrichment based on partition of unity. *International Journal for Numerical Methods in Engineering* 2005; **62**:1341–1359.
22. Wagner GJ, Ghosal S, Liu WK. Particulate flow simulations using lubrication theory solution enrichment. *International Journal for Numerical Methods in Engineering* 2003; **56**:1261–1289.
23. Chessa J, Belytschko T. An enriched finite element method and level sets for axisymetric two-phase flow with surface tension. *International Journal for Numerical Methods in Engineering* 2003; **58**:2041–2064.
24. Sukumar N, Hang Z, Prevost JH, Suo Z. Partition of unity enrichment for bimaterial interface cracks. *International Journal for Numerical Methods in Engineering* 2004; **59**:1075–1102.
25. Aragón AM, Duarte CA, Geubelle PH. Generalized finite element enrichment functions generalized finite element enrichment functions for discontinuous gradient fields. *International Journal for Numerical Methods in Engineering* 2010; **82**:242–268.
26. Moës N, Cloirec M, Cartraud P, Remacle JF. A computational approach to handle complex microstructure geometries. *Computer Methods in Applied Mechanics and Engineering* 2003; **192**:3163–3177.
27. Moës N, Béchet E, Tourbier M. Imposing Dirichlet boundary conditions in the extended finite element method. *International Journal for Numerical Methods in Engineering* 2006; **67**(12):1641–1669.
28. Babuška I, Banerjee U, Osborn JE. Survey of meshless and generalized finite element methods: a unified approach. *Acta Numerica* 2003; **12**:1–125.
29. Fries TP. A corrected XFEM approximation without problems in blending elements. *International Journal for Numerical Methods in Engineering* 2008; **75**(5):503–532.
30. Strouboulis T, Babuška I, Copps K. The design and analysis of the generalized finite element method. *Computer Methods in Applied Mechanics and Engineering* 2000; **181**:43–69.
31. Zienkiewicz OC, Taylor RL, Zhu JZ. *The Finite Element Method: Its Basis and Fundamentals*. Elsevier: Heinemann, 2005.

DOI: 10.1002/nme

32. Li Z, Lin T, Wu X. New cartesian grid methods for interface problems using the finite element formulation. *Numerische Mathematik* 2003; **96**:61–98.
33. Srinivasan KR, Matouš K, Geubelle PH. Generalized finite element method for modeling nearly incompressible bimaterial hyperelastic solids. *Computer Methods in Applied Mechanics and Engineering* 2008; **197**:4882–4893.
34. Toohey KS, Sottos NR, Lewis JA, Moore JS, White SR. Self-healing materials with microvascular networks. *Nature Materials* 2007; **6**:581–585.
35. Olugebefola SC, Aragón AM, Hansen CJ, Hamilton AR, Kozola BD, Wu W, Geubelle PH, Lewis JA, Sottos NR, White SR. Polymer microvascular network composite. *Journal of Composite Materials* 2010; **44**(22):2587–2603.
36. Golden AP, Tien J. Fabrication of microfluidic hydrogels using molded gelatin as a sacrificial element. *Lab on a Chip* 2007; **4**(6):720–725.
37. Aragón AM, Wayer JK, Geubelle PH, Goldberg DE, White SR. Design of microvascular flow networks using multi-objective genetic algorithms. *Computer Methods in Applied Mechanics and Engineering* 2008; **197**:4399–4410.
38. Brebbia CA, Ferrante A. *Computational Hydraulics*. Butterworths: London, 1983.

DOI: 10.1002/nme